Electronic Supplementary Material (ESI) for ChemComm.

The table of contents entry

Keyword: tandem dye-sensitized solar cells

Christopher J. Wood, Gareth H. Summers, Elizabeth A. Gibson*

Increased photocurrent in tandem dye-sensitized solar cell by modifications in push-pull dye-design.

New donor-π-acceptor dyes functionalised with a bodipy or indolium acceptor are described, which have an excellent spectral response in the red region and generate record photocurrent in tandem dye-sensitized solar cells. Our cationic acceptor dye, CAD3, generated a cathodic photocurrent density of 8.2 mA cm^{-2}, the highest reported for a NiO p-type solar cell to date.

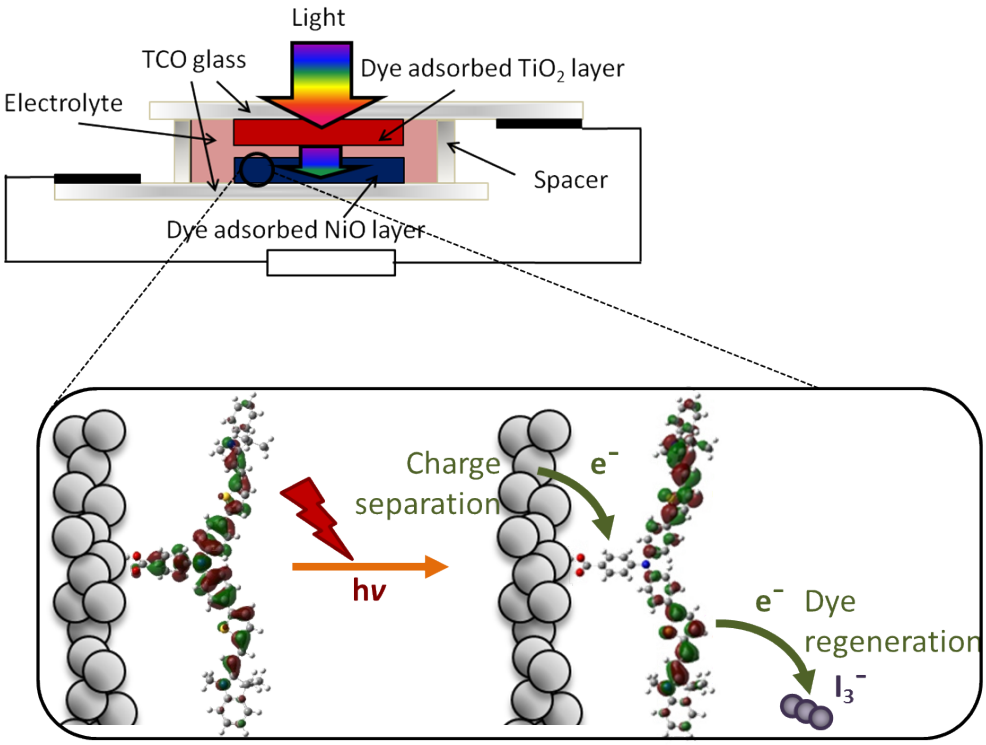

Supporting Information

Increased photocurrent in tandem dye-sensitized solar cell by modifications in push-pull dye-design.

*Christopher J. Wood, Gareth H. Summers, Elizabeth A. Gibson**

Contents

Table S4. Comparison of calculated energies of the frontier molecular orbitals of [**CAD3**]$^+$**,** calculated using B3LYP (6-31G(d)) and CAM-B3LYP (6-31+G(d)) in dichloromethane using the polarisable continuum model (PCM) solvation model.
Table S5. Comparison of TDDFT data for [**CAD3**]$^+$**,** calculated using TD-B3LYP (6-31G(d)) and TD-CAM-B3LYP (6-31+G(d)) in dichloromethane using the polarisable continuum model (PCM) solvation model. Percentage contributions were calculated from %=200C^2, where C is the given contribution.
Figure S13. Comparison of the calculated electron distirbutions of the frontier molecular orbitals of [**CAD3**]$^+$**,** calculated using B3LYP (6-31G(d)) and CAM-B3LYP (6-31+G(d)) in dichloromethane using the polarisable continuum model (PCM) solvation model.

Solar Cell Characterisation Data
Figure S14. Current-voltage plots for NiO p-DSCs sensitized with the dyes **CAD3** (triangles), **GS1** (circles) and **P1** (diamonds), assembled with a platinised counter electrode and infiltrated with triiodide/iodide electrolyte.
Figure S15. Dark current plots for NiO p-DSCs sensitized with the dyes **CAD3** (triangles), **GS1** (circles) and **P1** (diamonds), assembled with a platinised counter electrode and infiltrated with triiodide/iodide electrolyte.
Figure S16. IPCE plots for NiO p-DSCs sensitized with the dyes **CAD3** (triangles), **GS1** (circles) and **P1** (diamonds) assembled with a platinised counter electrode and infiltrated with triiodide/iodide electrolyte.
Figure S17. Dye loading plots for multi-layered NiO films sensitized with the dyes **CAD3** (triangles), **GS1** (circles) and **P1** (diamonds).
Figure S18. Current-voltage plots for TiO_2 n-DSCs sensitized with the dye **D35** using different dilutions of TiO_2 paste in ethanol, **2(EtOH):1(TiO_2 paste)** (diamonds), **2.5:1** (circles), **3:1** (squares), **3.5:1** (triangles) assembled with a platinised counter electrode and infiltrated with triiodide/iodide electrolyte.
Figure S19. Dark current plots for TiO_2 n-DSSCs sensitized with the dye **D35** using different dilutions of TiO_2 paste in ethanol, **2(EtOH):1(TiO_2 paste)** (diamonds), **2.5:1** (circles), **3:1** (squares), **3.5:1** (triangles), assembled with a platinised counter electrode and infiltrated with triiodide/iodide electrolyte.
Figure S20. IPCE plots for TiO_2 n-DSSCs sensitized with the dye **D35** using different dilutions of TiO_2 paste in ethanol, **2(EtOH):1(TiO_2 paste)** (diamonds), **2.5:1** (circles), **3:1** (squares), **3.5:1** (triangles), assembled with a platinised counter electrode and infiltrated with triiodide/iodide electrolyte.
Figure S21. Current-voltage plots for for Tandem DSCs sensitized by **D35/CAD 3** (triangles), **D35/GS01** (circles) **and D35/P1** (diamonds)
Figure S22. Dark current plots for Tandem DSCs sensitized by **D35/CAD3** (triangles), **D35/GS1** (circles) and **D35/P1** (diamonds).
Figure S23. Relative potential energy levels of **P1**, **GS1**, **CAD3**.

Structure of D35

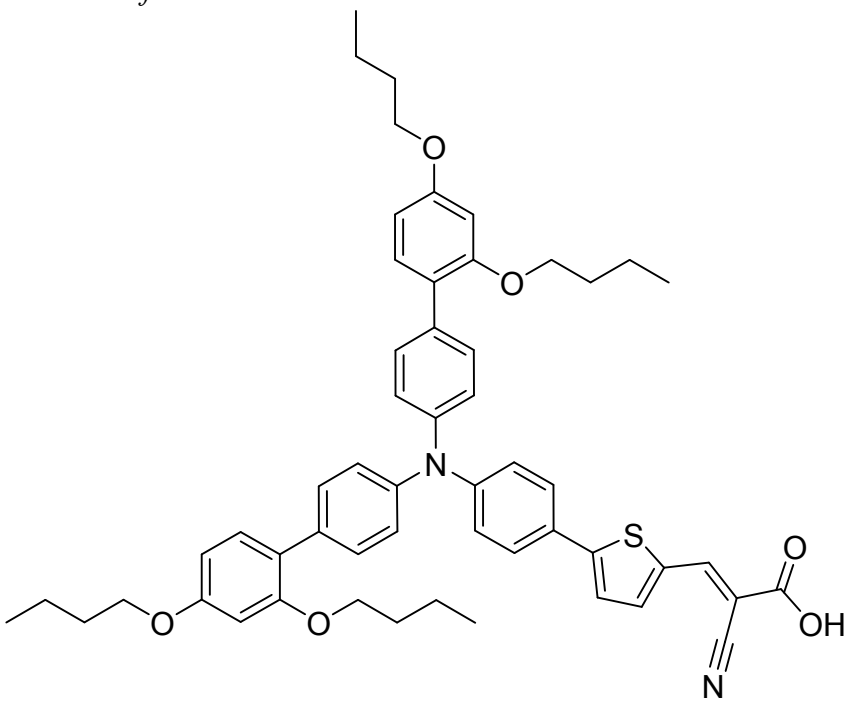

Figure S1. Structure of **D35** used to sensitize TiO_2 in this study.

Experimental Section

Analytical Measurements

^{1}H and ^{13}C NMR HMQC, HMBC and COSY NMR spectra were recorded using a Bruker DPX 300 and a Bruker AV(III) 400. Mass spectra were recorded using a Bruker microTOF mass spectrometer. UV-visible absorption spectroscopy measurements in solution were recorded on either a Perkin Elmer Lambda 25 UV-Vis spectrometer or an Ocean Optics USB2000+ VIS-NIR fibre optic spectrometer. The magnitude of the zero−zero singlet transition (E_{0-0}) was estimated from the point of intercept of the normalised absorption and emission spectra [E_{0-0} (eV) = $1240/\lambda_{inter}$ (nm)]. Electrochemical oxidation and reduction potentials were obtained by cyclic voltammetry (CV) or differential pulse voltammetry on a Palmsens Emstat potentiostat. A three electrode system was used with a glassy carbon disk working electrode, Pt wire counter electrode and a $AgNO_3/Ag$ reference electrode. The supporting electrolyte was 0.1 M Bu_4NClO_4 in dichloromethane or acetonitrile. For all electrochemical techniques the values were calibrated against a $Fe(Cp)_2^{+/0}$ external standard.

DFT calculations

DFT calculations were carried out using Gaussian G03[6] on the University of Nottingham Minerva HPC at a B3LYP/6-31G(d) and Gaussian G09[7] at a CAM-B3LYP/6-31G+(d) level of theory using the polarisable continuum solvation model for dichloromethane. A methyl group was used to replace the hexyl groups in CAD3 to reduce computational expense and the PF_6^- counter ion was not included in the calculation. Energies and isodensity surfaces of the highest occupied molecular orbitals (HOMOs) and lowest unoccupied molecular orbitals (LUMOs) were then calculated. Time-dependent DFT (TDDFT) calculations were then carried out at a B3LYP/6-31G(d) level of theory in dichloromethane on the optimised geometries to calculate simulated optical absorption spectra. As B3LYP 6-31G(d) underestimates the energy of the charge transfer electronic transitions we also tested our calculations using CAM-B3LYP 6-31G+(d).[8] The results are presented in Table 4, 5 and Figure S13 for comparison.

Solar Cells

Conducting glass substrates were cut to size and then by cleaned in an ultrasonic bath for 15 minutes, first in soapy water, second in iso-propanol and finally in acetone. NiO precursor solution was prepared by dissolving anhydrous $NiCl_2$ (1 g) and the tri-block co-polymer F108 (poly (ethylene glycol)-*block*-poly (propylene glycol)-*block*-poly (ethylene glycol)) (1 g) in ethanol (6 g) and ultrapure Milli-Q water (5 g).[1] NiO electrodes were made by applying the precursor solution onto conducting glass substrates (Pilkington TEC15, sheet resistance 15 Ω/square) by doctor blade using Scotch tape as a spacer (0.2 cm^2 active area), followed by sintering in a Nabertherm B150 oven at 450 °C for 30 min. The NiO electrodes were soaked in an acetonitrile solution of **P1** or a dichloromethane solution of **GS1** or **CAD3** (0.3 mM) for 16 h at room temperature. The dyed NiO electrodes were assembled face-to-face with a

platinized counter electrode (Pilkington TEC8, sheet resistance 8 Ω/square) using a 30 μm thick thermoplastic frame (Surlyn 1702). The electrolyte, containing LiI (1.0 M) and I_2 (0.1 M) in acetonitrile, was introduced through the pre-drilled hole in the counter electrode, which was sealed afterwards. For the dye adsorption studies 0.2 cm^2 NiO films were immersed in dye solutions and the absorbance of the solution was recorded after 24 h. TiO_2 electrodes (0.2 cm^2 active area) were made by pre-treating the TEC 15 conducting glass substrates in aqueous $TiCl_4$ solution (40 mM) at 70 ºC for 45 minutes. The conducting glass substrates were then rinsed with water and acetone and then allowed to dry before annealing in a Nabertherm B150 oven at 450 °C for 30 min. Commercial TiO_2 paste (Solaronix, Ti-nanoxide T/SP) diluted with ethanol (2(EtOH):1(TiO_2 paste), 2.5:, 3:1, 3.5:1 by weight), was applied, followed by sintering in a Nabertherm B150 oven at 450 °C for 30 min. The electrodes were then post-treated by immersing in $TiCl_4$ solution (40 mM) at 70 ºC for 45 minutes and annealing in a Nabertherm B150 oven at 450 °C for 30 min. The TiO_2 electrodes were soaked in an ethanol solution of D35 (Dyenamo AB) (0.3 mM) for 8 h at room temperature. Solar cell assembly was performed as described above with an electrolyte containing LiI (1.0 M) and I_2 (0.1 M) in acetonitrile. Current-voltage measurements were measured using an Ivium CompactStat potentiostat under AM 1.5 simulated sunlight from an Oriel 150 W solar simulator, giving light with an intensity of 100 mW cm^{-2}. Incident photon-to-current conversion efficiencies were recorded by passing the light from the solar simulator through an Oriel Cornerstone 130 1/8m monochromator and recording the current from the solar cell with an Ivium CompactStat potentiostat which was calibrated against a Si photodiode.

Synthesis

All reagents and anhydrous solvents were purchased from Sigma-Aldrich. P1 was prepared using a modified procedure first reported by Qin *et al.*[2] Diphenyliodonium triflate was

prepared according to the procedure by Bielawski *et al.*[3] 2-phenyl-1H-pyrrole was prepared according to the procedure by Wen *et al.*[4] 1-hexyl-2,3,3-trimethyl-3H-indolium hexafluorophosphate was prepared according to the procedure by Tyler *et al.*[5] The hexafluorophosphate anion instead of the bromide was selected for ease of purification by size exclusion chromatography.

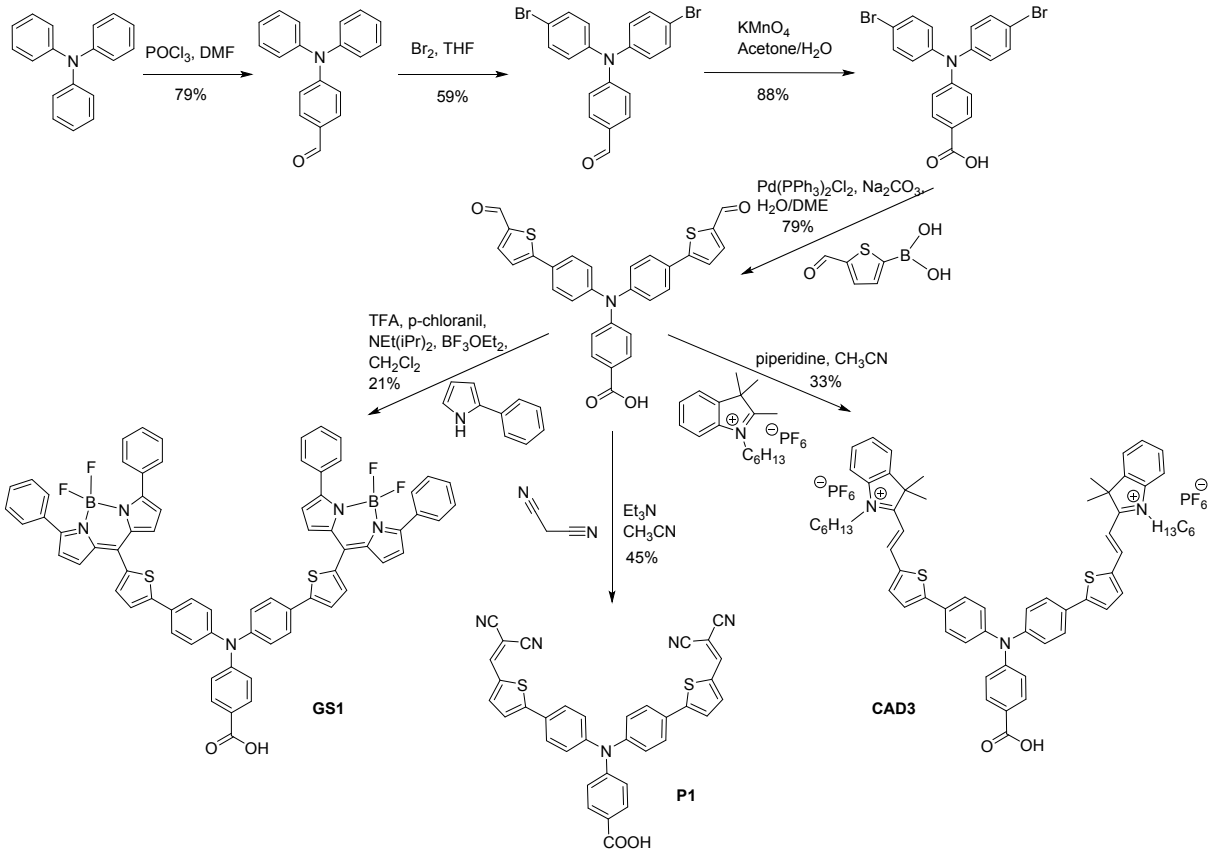

Figure S2. General reaction scheme for **P1**, **GS1** and **CAD3**.

4-formyltriphenylamine

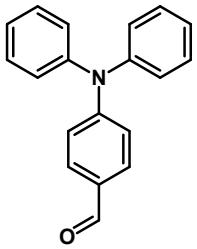

Triphenylamine (10 g, 40 mmol) was dissolved in anhydrous N,N-Dimethylformamide (100 mL) under nitrogen and the solution was cooled to 0°C with stirring. Phosphoryl chloride

(1.95 mL, 0.21 mol, 5.25 eqv.) was added slowly to the solution and then this was warmed to 100°C and stirred for 5 hours under nitrogen. After allowing to cool to room temperature, the mixture was neutralised using a 2 M sodium hydroxide solution. After stirring for a further 30 minutes, the mixture was extracted with ethyl acetate (3 x 200 mL), the organic layer dried with magnesium sulfate and then the solution evaporated under reduced pressure. The crude residue was then purified by silica gel chromatography (using a 2:1 heptane/chloroform eluent) to afford 8.75 g of the product as a beige solid in 79% yield.

^{1}H NMR (300 MHz, $CDCl_3$, δ): 9.82 (s, 1H, CHO), 7.69 (d, J = 8.7 Hz, 2H, Ar H), 7.41-7.30 (m, 4H, Ar H), 7.24-7.13 (m, 6H, Ar H), 7.03 (d, J = 8.7 Hz, 2H, Ar H); HRMS (ESI+ TOF) *m/z*: $[M+H]^+$ calcd for $C_{19}H_{16}NO$, 274.12; found: 274.12.

4,4'-dibromo-4''-formyltriphenylamine

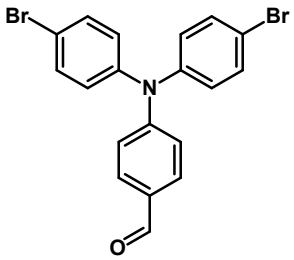

4-formyltriphenylamine (1 g, 3.659 x 10^{-3} mol) was dissolved in anhydrous dichloromethane (40 mL) under nitrogen. The reaction mixture was cooled to 0°C and bromine (0.375 mL, 7.317 x 10^{-3} mol, 2 eqv.) was added dropwise under a flux of nitrogen. The mixture was stirred at room temperature for 6 hours and monitored by TLC. The reaction was then quenched with aqueous potassium hydroxide, extracted with dichloromethane (3 x 30 mL), the organic phase washed with deionised water (3 x 20 mL) and then dried with magnesium sulfate and evaporated under reduced pressure. The crude residue was then purified by silica gel chromatography (using a pentane:DCM gradient as the eluent) to afford 930 mg of the product as a yellow solid in 59% yield.

^{1}H NMR (300 MHz, $CDCl_3$, δ): 9.85 (s, 1H, CHO), 7.72 (d, 2H, J = 8.8 Hz, Ar H), 7.46 (d, 2H, J = 8.8 Hz, Ar H), 7.05 (m, 6H, Ar H); HRMS (ESI+ TOF) *m/z*: $[M+H]^+$ calcd. for $C_{19}H_{14}Br_2NO$: 429.94, found: 429.94.

4-[bis-(4-bromo-phenyl)-amino]-benzoic acid

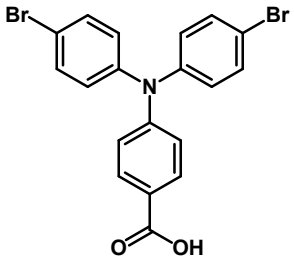

4,4'-dibromo-4''-formyltriphenylamine (250 mg, 5.799 x 10^{-4} mol) was suspended in an acetone/water mixture (3:1 v/v, 45/15 mL) and the mixture was heated to reflux. Potassium permanganate (368 mg, 2.329 x 10^{-3} mol, 4 eqv.) was slowly added portion wise to the solution over the course of an hour and then the mixture was heated at reflex for four hours. After allowing to cool to room temperature, the acetone was evaporated and then the mixture was diluted with water (40 mL). The solution was filtered to remove any precipitate, this precipitate washed with water and then the collected filtrate was acidified with concentrated hydrochloric acid until precipitation occurred. This precipitate was filtered, washed with water and dried under a flux of air to afford 165 mg of the product as a white solid in 62 % yield.

^{1}H NMR (300 MHz, $CDCl_3$, δ): 7.94 (d, J = 8.7 Hz, 2H, Ar H), 7.43 (d, J = 8.7 Hz, 4H, Ar H), 7.04-6.98 (m, 6H, Ar H); HRMS (ESI– TOF) *m/z*: $[M–H]^-$ calcd for $C_{19}H_{12}Br_2NO_2$: 443.92, found: 443.92.

4-carboxy-4',4''-di-(5-formyl-2-thienyl)Triphenylamine

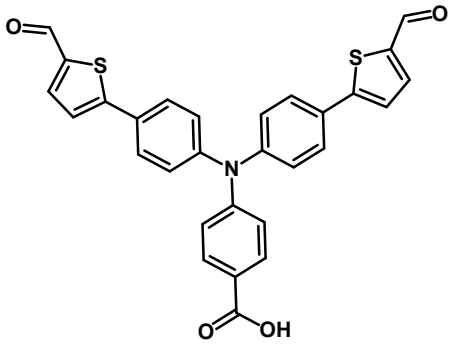

4-[bis-(4-bromo-phenyl)-amino]-benzoic acid (163 mg, 3.650 x 10^{-4} mol), 5-formyl-2-thienylboronic acid (150 mg, 9.617 x 10^{-4} mol, 2.6 eqv.), bis-triphenylphosphinepalladium(II) chloride (13 mg, 1.852 x 10^{-5} mol, 0.05 eqv.) and sodium carbonate (192 mg, 1.811 x 10^{-3} mol, 5 eqv.) were loaded into a Schlenk tube and purged with nitrogen. The reagents were dissolved in a H_2O/1,2-dimethoxyethane mixture (1:6 v/v, .5/3 mL) and this was heated to 90°C overnight. After cooling to room temperature, the reaction mixture was diluted with water (3 mL) and acidified with 0.1M hydrochloric acid until a slightly acidic pH was achieved. The mixture was extracted with ethyl acetate (3 x 20mL), the organic phase washed with water (3 x 5mL), dried with magnesium sulfate and then evaporated under reduced pressure. The crude product was then purified by silica gel chromatography (using a DCM:methanol gradient as the eluent) to afford 121 mg of the product as a yellow solid in 65% yield.

^{1}H NMR (300 MHz, $CDCl_3$, δ): 9.91 (2H, s, CHO), 8.02 (2H, d, J = 8.7 Hz, Ar H), 7.77 (2H, d, J = 4.3 Hz, thiophene), 7.65 (4H, d, J = 8.7 Hz, Ar H), 7.40 (2H, d, J= 4.3 Hz, thiophene), 7.22 (4H, d, J = 8.8 Hz, Ar H), 7.17 (2H, d, J = 8.8 Hz, Ar H); HRMS (ESI– TOF) *m/z*: $[M–H]^-$ calcd. for $C_{29}H_{18}NO_4S_2$: 508.07, found: 508.07.

P1

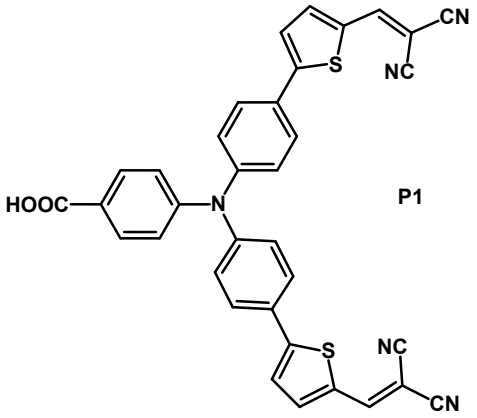

4-carboxy-4',4''-di-(5-formyl-2-thienyl)triphenylamine (27 mg, 5.30 x 10^{-5} mol, 1 eqv.) was loaded into a Schlenk tube and purged with nitrogen followed by the addition of anhydrous acetonitrile (10 mL). Malononitrile (7.5 mg, 1.13 x 10^{-4} mol, 2.1 eqv.) and four drops of triethylamine were added. The mixture was refluxed at 90°C for 2 hours. After cooling to room temperature, the solution was extracted into DCM (3 x 10 mL), washed with water (3 x 10 mL), dried using magnesium sulfate and the solvent evaporated. The crude residue was purified by column chromatography using a DCM/methanol (v/v 99.5/0.5) eluent to give 14.5 mg of the product as a red solid in 45% yield.

^{1}H NMR (300 MHz, $CDCl_3$, δ): 8.03 (2H, d, J = 8.4 Hz, Ar-H), 7.81 (2H, s, $CHC(CN)_2$), 7.74 (2H, d, J = 3.80 Hz, thiophene), 7.67 (4H, d, J = 8.40 Hz, Ar-H), 7.43 (2H, d, J = 3.80 Hz, thiophene), 7.22 (6H, m, Ar-H); HRMS (ESI– TOF) *m/z* : $[M–H]^-$ calcd. for $C_{35}H_{18}N_5O_2S_2$: 604.09, found: 604.09.

Diphenyliodonium triflate

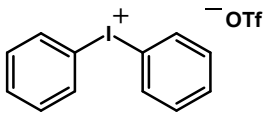

3-Chloroperbenzoic acid (308 mg, 1.785 x 10^{-3} mol, 1.1 eqv.) was added to a solution of iodobenzene (0.180 mL, 1.608 x 10^{-3} mol, 1 eqv.) in dichloromethane (10 mL). Benzene was

added (0.157 mL, 1.757 x 10^{-3} mol, 1.1 eqv.) followed by the dropwise addition of trifluoromethanesulfonic acid (0.428 mL, 4.837 x 10^{-3} mol, 3 eqv.) The reaction mixture was stirred at room temperature for 30 minutes before concentrating under vacuum. The addition of diethyl ether resulted in the precipitation of the product to afford 527 mg of white solid in 68% yield.

^{1}H NMR (300 MHz, $CDCl_3$, δ): 8.37 (d, 4H, J = 7.4 Hz, Ar H), 7.80 (t, 2H, J = 7.4 Hz, Ar H), 7.64 (t, 4H, J = 7.4 Hz, Ar H) ppm; HRMS (ESI+ TOF) *m/z*: $[M]^+$ calcd. for $C_{13}H_{11}F_3IO_3S$: 430.94, found: 280.98.

2-phenyl-1H-pyrrole

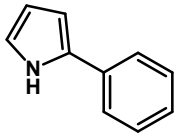

Diphenyliodonium triflate (527 mg, 1.225 x 10^{-3} mol, 1 eqv.) and sodium hydroxide (73.5 mg, 1.838 x 10^{-3} mol, 1.5 eqv.) were loaded into a Schlenk tube and purged with nitrogen. Pyrrole (2.5 mL) was added and the reaction mixture was heated at 80°C overnight. After cooling to room temperature, ethyl acetate was added (10 mL), the mixture was washed with water (3 x 5mL) and the organic phase dried using magnesium sulfate. The crude product was then purified by silica gel chromatography (using a 2:1 hexane/ethyl acetate eluent) to afford 121 mg of the product as a white solid in 69% yield.

^{1}H NMR (300 MHz, $CDCl_3$, δ): 8.46 (1H, s, Ar H), 7.50 (2H, d, J = 7.4 Hz, Ar H), 7.39 (2H, t, J = 7.5 Hz, Ar H), 7.25 (1H, dd, J = 15 Hz, 7.4 Hz, Ar H); HRMS (ESI+ TOF) *m/z*: $[M+H]^+$ calcd. for $C_{10}H_{10}N$: 144.08, found: 144.08.

GS1

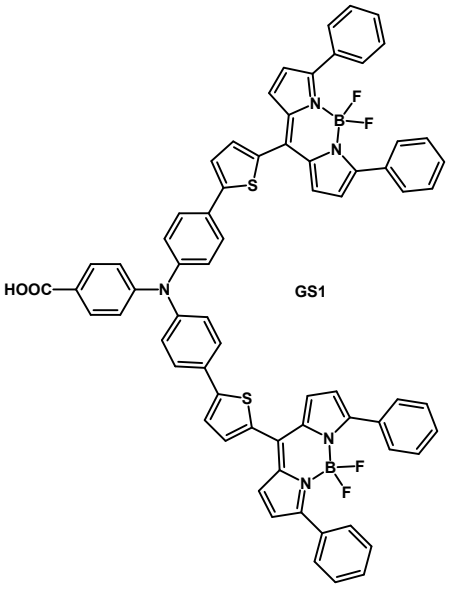

4-carboxy-4',4''-di-(5-formyl-2-thienyl)triphenylamine (47 mg, 9.22 x 10^{-5} mol) and 2-phenyl-1H-pyrrole (53.14 mg, 3.71 x 10^{-4} mol, 4.02 eqv.) were loaded into a Schlenk tube purged with nitrogen and then dissolved in anhydrous dichloromethane (15 mL). 1 drop of trifluoroacetic acid was added and the mixture was stirred at room temperature overnight. p-chloranil (47 mg, 1.91 x 10^{-4} mol, 4.02 eqv.) was added under a flux of nitrogen and the solution was stirred for a further 30 minutes. Diisopropylethylamine (0.192 mL, 1.10 x 10^{-3} mol, 12 eqv.) was added via syringe and the reaction was stirred for another 10 minutes before adding boron trifluoride etherate (0.228 mL, 1.84 x 10^{-3} mol, 20 eqv.) and stirring for four hours. The reaction mixture was washed with water (3 x 10 mL), dried using magnesium sulfate and evaporated under reduced pressure. The crude product was purified by silica gel chromatography (using a DCM:methanol gradient as the eluent) to afford the product as a purple solid which was recrystallised with a dichloromethane/pentane mixture to afford 22.5 mg of the product in 21% yield.

^{1}H NMR (300 MHz, $CDCl_3$, δ): 7.95 (2H, d, J = 8.75 Hz, Ar H), 7.79 (8H, dd, J = 10, 3 Hz, Ar H) 7.61 (4H, d, J = 8.5 Hz, Ar H), 7.49 (2H, d, J = 3.5 Hz, thiophene), 7.38 (2H, d, J = 3.5 Hz, thiophene), 7.36 (4H, d, J = 2 Hz, Ar H), 7.34 (8H, d, J = 2 Hz, Ar H), 7.29 (4H, d, J = 4.5 Hz, pyrrole), 7.17 (4H, d, J = 8.5 Hz, Ar H), 7.12 (2H, d, J = 8.75 Hz, Ar H), 6.62 (4H, d, J =

4.5 Hz, pyrrole); ^{13}C NMR (700 MHz, $CDCl_3$, δ): 158.8, 151.5, 149.0, 147.1, 146.7, 136.2, 135.7, 134.1, 133.7, 132.8, 132.7, 130.6, 129.6, 129.5, 128.2, 127.4, 125.8, 123.8, 121.7, 120.9, 119.1; ^{11}B NMR (96 MHz, $CDCl_3$, δ): 1.33 (t, J = 30 Hz); ^{19}F NMR (282 MHz, $CDCl_3$, δ): -132.35 (q, J = 32 Hz); HRMS (MALDI-TOF) *m/z*: $[M+H]^+$ calcd. for $C_{69}H_{46}B_2F_4N_5O_2S_2$: 1138.32, found: 1138.88.

1-hexyl-2,3,3-trimethyl-3H-indolium hexafluorophosphate

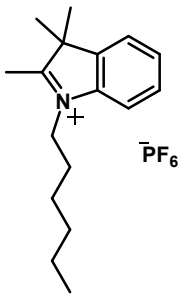

2,3,3-trimethyl-3H-indole (5 g, 31 x 10^{-3} mol) and 1-bromohexane (6.2 g, 38 x 10^{-3} mol) were dissolved in acetonitrile (30 mL) and refluxed under nitrogen for 12 h. The solvent was evaporated and the crude product was washed with diethyl ether three times. A portion of the crude product (1.46g, 3.65 x 10^{-3} mol) and excess $NaPF_6$ (1.51 g, 8.9 x 10^{-3} mol) were then dissolved in methanol (10 mL). The mixture was stirred for 3 hours. The solvent was then evaporated and the product was recrystallized from DCM:Pentane to give of a light purple solid(1.25 g, 2.34 x 10^{-3} mol).

^{1}H NMR (400 MHz, CD_3CN, δ): 7.76 (m, 2H, Ar H), 7.66 (m, 2H, Ar H), 4.38 (t, *J* = 7.9 Hz, 2H, CH_2), 2.75 (s, 3H, CH_3), 1.58 (s, 6H, CH_3), 1.58-1.21 (m, 8H, CH_2), 0.94 (t, *J* = 6.86 Hz, 3H, CH_3); ^{13}C NMR (75 MHz, CD_3CN, δ): 129.93, 129.08, 123.45, 115.32, 54.59, 48.22, 30.92, 27.36, 25.81, 22.08, 21.67, 13.63, 13.20; ^{31}P NMR (CD_3CN, 121 MHz, δ): -144.62 (sep, J_{PF}=705 Hz, 1P); ^{19}F NMR (CD_3CN, 282 MHz, δ): -72.84 (d, J_{FP}=707 Hz, 6F); HRMS (ESI+ TOF) *m/z*: $[M]^+$ calcd for $C_{17}H_{26}N^+$, 244.2060; found 244.2065.

CAD3

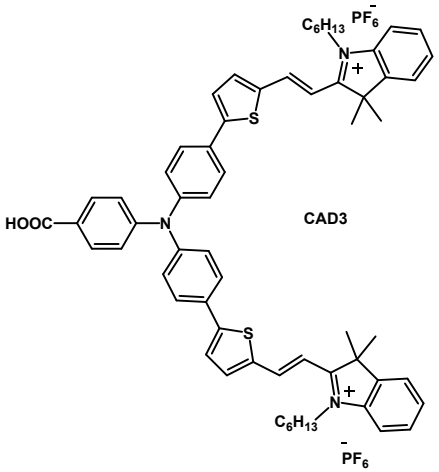

1-hexyl-2,3,3-trimethyl-3H-indolium hexafluorophosphate (150 mg, 3.85 x 10^{-4} mol) and 4-Carboxy-4',4''-di(5-formyl-2-thienyl)triphenylamine (50 mg, 9.8 x10^{-5} mol) were added to CH_3CN (5 ml) and refluxed for 12 h, with piperidine (15 µl, 12.93 mg, 1.52 x 10^{-4} mol) as a catalyst. The product was precipitated from the reaction mixture by addition of water (~5 ml). The product was then recrystallized from DCM:Pentane to give a blue solid. The product was further purified by size exclusion chromatography on Sephadex LH-20 in CH_3CN to give 37 mg of the product in 33% yield.

^{1}H NMR (400 MHz, CD_3CN, δ): 8.47 (d, *J* = 15.8 Hz, 2H, Ar H), 7.99 (d, *J* = 8.3 Hz, 2H, Ar H), 7.96 (d, *J* = 4.3, 2H, thiophene), 7.81 (d, *J* = 8.7 Hz, 4H, Ar H), 7.60 (d, *J* = 4.2, 2H, thiophene), 7.60-7.77 (m, 8H, Ar H), 7.27 (d, *J* = 8.3 Hz, 4H, Ar H), 7.21 (d, 8.3 Hz, 2H, Ar H), 7.06 (d, *J* = 15.7 Hz, 2H, Ar H), 4.46 (t, *J* = 7.6 Hz, 4H, CH_2), 1.94 (m, CH_2, 4H), 1.82 (s, 12H, CH_2CH_3), 1.30-1.57 (m, CH_2, 12H), 0.93 (t, *J* = 7.3 Hz, 6H, CH_3); ^{13}C NMR (75 MHz, CD_3CN, δ): 209.49, 189.36, 180.70, 154.34, 148.09, 147.81, 147.43, 140.08, 139.06, 129.33, 127.76, 126.05, 125.28, 123.18, 122.89, 119.60, 109.26, 64.93, 54.33, 52.25, 30.99, 29.89, 28.05, 25.95, 25.61, 22.15, 13.26; ^{31}P NMR (121 MHz, CD_3CN, δ): -144.63 (sep, J_{PF}=706 Hz, 1P); ^{19}F NMR (282 MHz, CD_3CN, δ): -72.92 (d, J_{FP}=706 Hz, 6F); HRMS (ESI+ TOF) *m/z*: $[M]^{2+}$ calcd for $C_{63}H_{67}S_2O_2N_3^{2+}$, 480.7332; found 480.7319.

Optical and Electrochemical Properties of P1, CAD3, GS1

Dye	Absorption			$E_{0\text{-}0}$ (eV)[c]	$E_{(D/D^-)}$ (V vs. $Fe(Cp)_2^{+/0}$)
	λ_{max}[a] (nm)	ε at λ_{max}[a] (L mol^{-1} cm^{-1})	λ_{max} on NiO[b] (nm)		
CAD3	614	94 580	566	1.78	-0.99[e]
GS1	565	65 700	565	2.11	-1.25[d]
P1	481	57 900	487	2.25	-1.46[e]

[a]Absorption and emission spectra were measured in dichloromethane solution at room temperature; [b]Absorption spectra of the dye adsorbed on a NiO film from a dichloromethane dye solution; [c] E_{0-0} was estimated from the intercept of the normalised absorption and emission spectra; [d] the reduction potential of GS1 was measured in acetonitrile with 100 mM (Bu_4NClO_4) supporting electrolyte (working electrode: glassy carbon; reference electrode: Ag^+/Ag calibrated with $Fe(Cp)_2^{+/0}$ as an internal reference, counter electrode: Pt). The reduction potential measured in dichloromethane solution was -1.29 V vs. $Fe(Cp)_2^{+/0}$ [e] the reduction potential of P1 and CAD3 were measured in dichloromethane with 100 mM (Bu_4NClO_4) supporting electrolyte (working electrode: glassy carbon; reference electrode: Ag^+/Ag calibrated with $Fe(Cp)_2^{+/0}$ as an internal reference, counter electrode: Pt).

Table S1: Summary of the optical and electrochemical properties of the dyes **CAD3**, **GS1** and **P1**.

Absorption Spectra

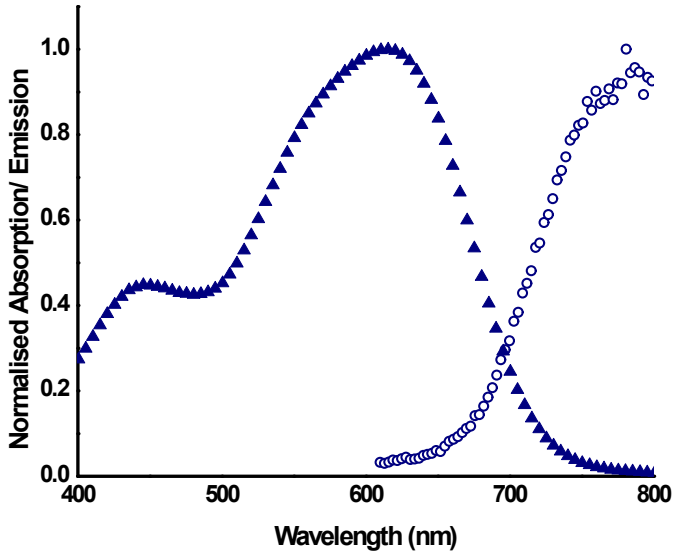

Figure S3. Absorption (triangles) and emission (open circles) spectra of **CAD3** in dichloromethane.

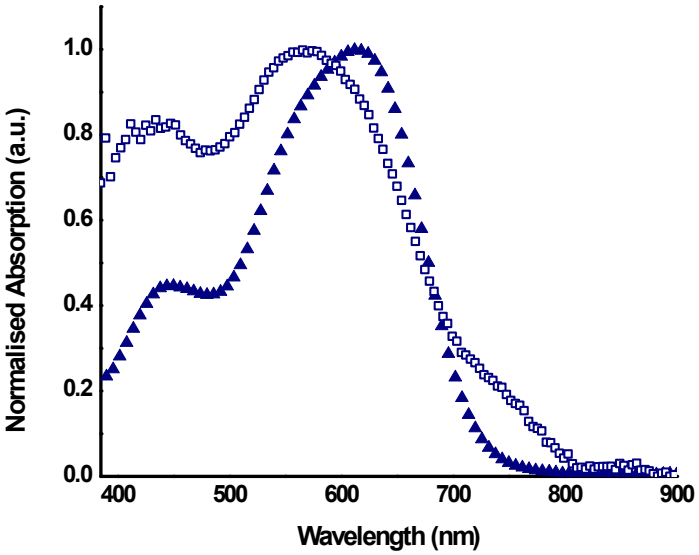

Figure S4. Absorption spectra of **CAD3** adsorbed on NiO (open squares) and in dichloromethane solution (triangles).

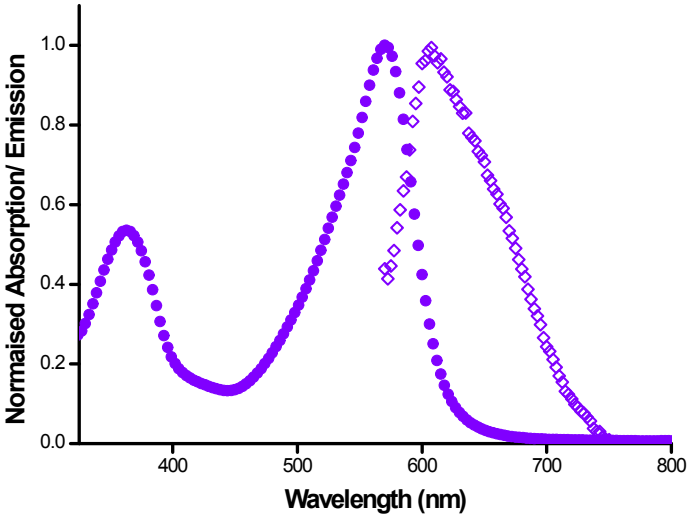

Figure S5. Absorption (circles) and emission (open diamonds) spectra of **GS1** in chloroform.

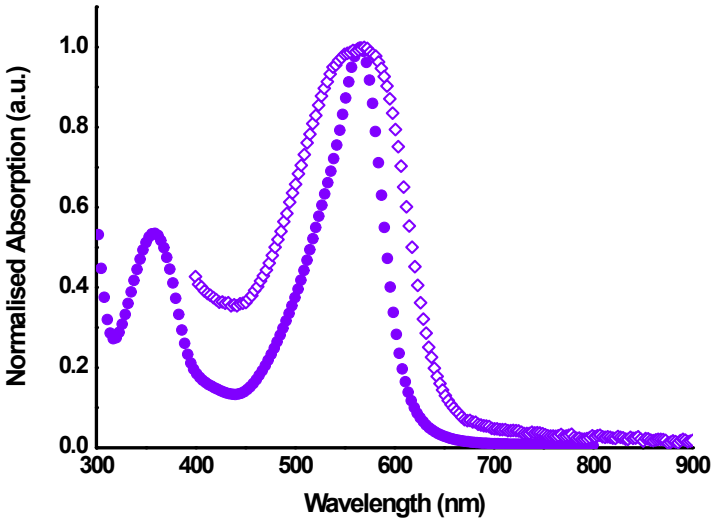

Figure S6. Absorption spectrum of **GS1** adsorbed on NiO (open diamonds) and in dichloromethane solution (circles).

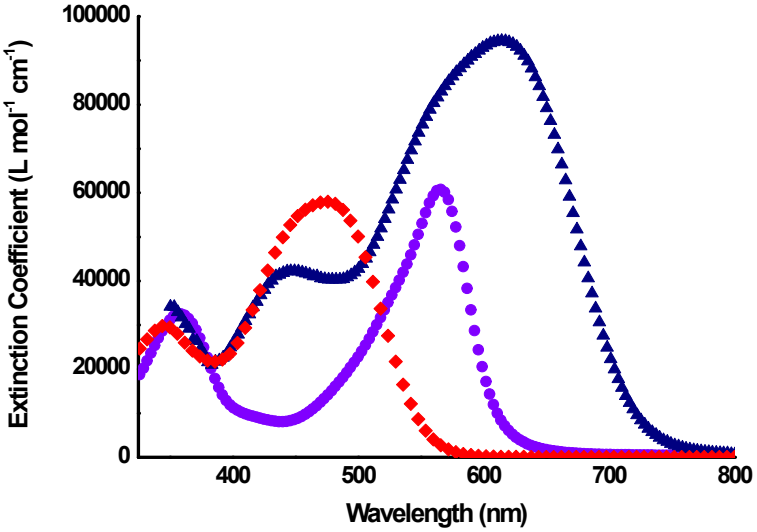

Figure S7. Absorption spectra of **CAD3** (triangles), **GS1** (circles) and **P1** (diamonds) in dichloromethane solution.

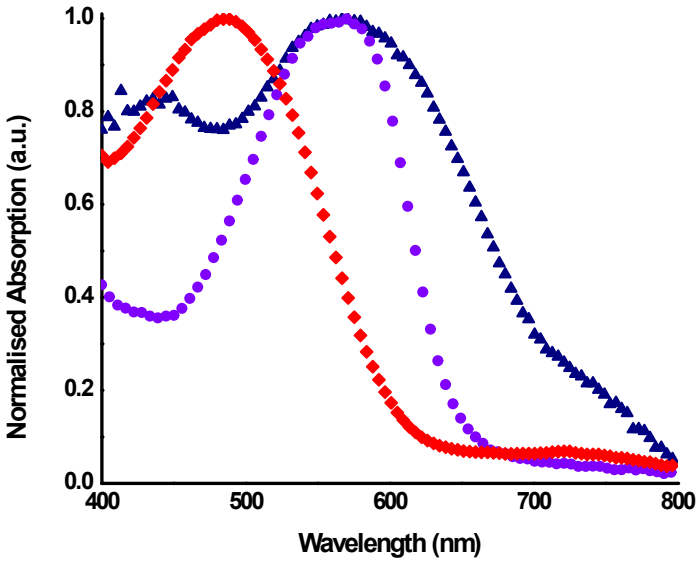

Figure S8. Normalised absorption spectra of **CAD3** (triangles), **GS1** (circles) and **P1** (diamonds) adsorbed onto NiO

Electrochemistry

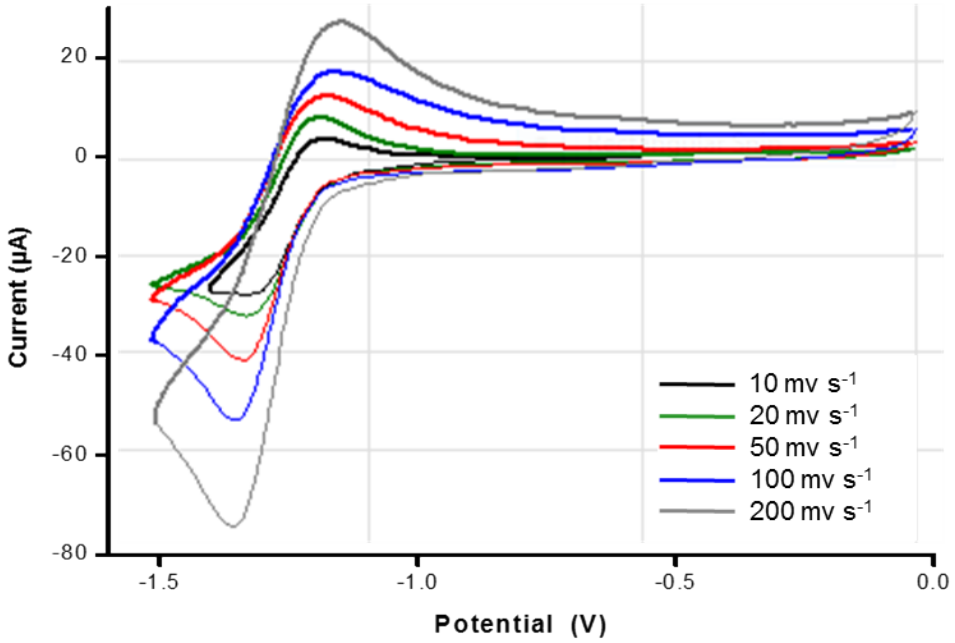

Figure S9. Cyclic voltammetry of **GS1** showing the reversible reduction. Cyclic voltammetry for GS1 was measured in acetonitrile with 100 mM (Bu_4NClO_4) supporting electrolyte (working electrode: glassy carbon; reference electrode: Ag^+/Ag calibrated with $Fe(Cp)_2^{+/0}$ as an internal reference, counter electrode: Pt).

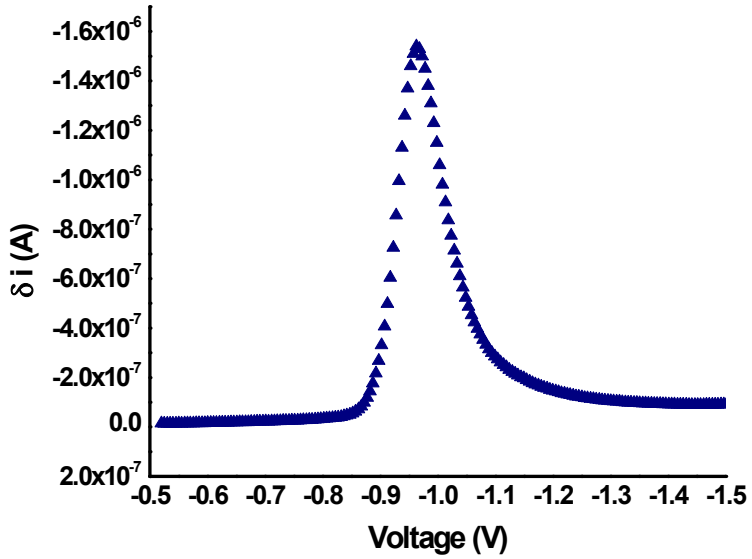

Figure S10. Differential pulse voltammetry for the reduction of **CAD3** measured in dichloromethane with 100 mM Bu_4NClO_4 as a supporting electrolyte (working electrode: glassy carbon; reference electrode: Ag/Ag^+; calibrated with ferrocene/ferrocenium $(Fe(Cp)^{+/0})$ as an internal reference, counter electrode: platinum wire).

Electronic Distribution Calculated Using Density Functional Theory

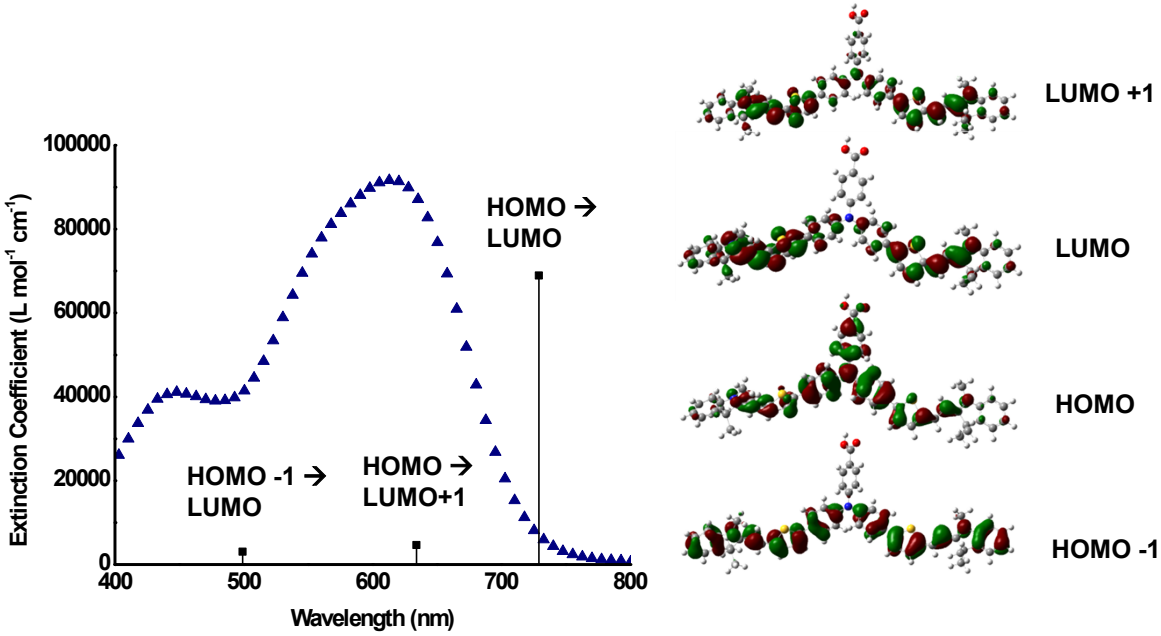

Figure S11. Comparison between the electronic transitions and their relative intensities calculated for [**CAD3**]$^+$ using TDDFT (B3LYP/6-31G(d)) with the experimentally determined UV−visible absorption spectra (left) for **CAD3**. Calculated electron distribution in the corresponding orbitals for [**CAD3**]$^+$ in dichloromethane using the polarisable continuum model (PCM) solvation model (right).[6]

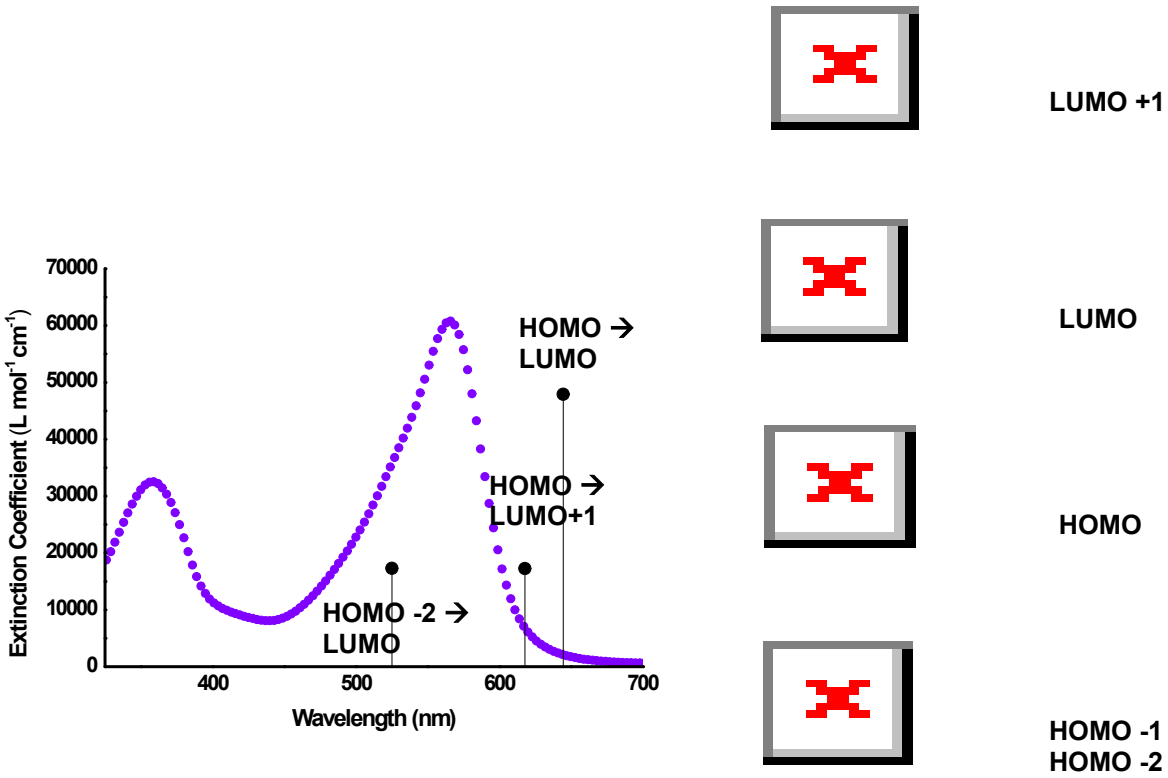

Figure S12. Comparison between the electronic transitions and their relative intensities calculated for **GS1** using TDDFT (B3LYP/6-31G(d)) with the experimentally determined

UV−visible absorption spectra (left) for **GS1**. Calculated electron distribution in the corresponding orbitals for **GS1** in dichloromethane using the polarisable continuum model (PCM) solvation model (right). The isodensity plots reveal that for **GS1** the electron density is found on the bridging thiophene in both the HOMO and LUMO, unlike in our previous dye (reference 4 in the main text) where the electron density was either exclusively located on the bodipy motif or on the triphenylamine-thiophene moiety.[6]

Dye	Molecular Orbital	Energy (eV)
[**CAD3**]$^+$	LUMO +1	-3.5697
	LUMO	-3.7007
	HOMO	-5.6872
	HOMO -1	-6.3675
GS1	LUMO +1	-2.8844
	LUMO	-2.9116
	HOMO	-5.1702
	HOMO -1	-5.4695

Table S2: Calculated energies of the frontier molecular orbitals of [**CAD3**]$^+$ and **GS1**, calculated using DFT (B3LYP/6-31G(d)) in dichloromethane using the polarisable continuum model (PCM) solvation model. [6]

Dye	Transition	λ (nm)	Oscillator Strength	Contribution
[**CAD3**]$^+$	HOMO →LUMO	729.21	2.0671	90.02 %
	HOMO → LUMO +1	643	0.1391	72.77 %
	HOMO +1 → LUMO	499.21	0.0910	85.43 %
GS1	HOMO → LUMO	644.60	0.6845	95.22 %
	HOMO → LUMO +1	617.87	0.2467	94.98 %
	HOMO -1 →LUMO	525.22	0.2470	13.23 %
	HOMO -1 → LUMO +1			2.46 %
	HOMO -2 → LUMO			43.87 %

Table S3: TDDFT data for [**CAD3**]$^+$ and **GS1,** calculated using DFT (B3LYP/6-31G(d)) in dichloromethane using the polarisable continuum model (PCM) solvation model. Percentage contributions were calculated from %=200C^2, where C is the given contribution. [6]

Comparison of B3LYP (6-31G(d)) and CAM-B3LYP (6-31G+(d)) basis sets for CAD3.

Basis Set	Molecular Orbital	Energy (eV)	Basis Set	Molecular Orbital	Energy (eV)
B3LYP (6-31G(d))			CAM-B3LYP (6-31G+(d))	LUMO +3	-1.01145
				LUMO +2	-1.10288
	LUMO +1	-3.5697		LUMO +1	-2.81856
	LUMO	-3.7007		LUMO	-2.92903
	HOMO	-5.6872		HOMO	-7.01428
	HOMO -1	-6.3675		HOMO -1	-7.72776
				HOMO -2	-8.16777

Table S4: Comparison of calculated energies of the frontier molecular orbitals of [**CAD3**]$^+$**,** calculated using B3LYP (6-31G(d)) and CAM-B3LYP (6-31+G(d)) in dichloromethane using the polarisable continuum model (PCM) solvation model.

Basis Set	Transition	λ (nm)	Oscillator Strength	Contribution
B3LYP (6-31G(d))	HOMO →LUMO	729.21	2.0671	90.02 %
	HOMO → LUMO +1	643	0.1391	72.77 %
	HOMO +1 → LUMO	499.21	0.0910	85.43 %
CAM-B3LYP (6-31G+(d))	HOMO -2 →LUMO HOMO →LUMO	537.88	3.2977	3.17 % 68.57 %
	HOMO-2 → LUMO +1 HOMO → LUMO +1	491.24	0.1827	5.51 % 58.61 %
	HOMO -2 → LUMO HOMO -1 → LUMO HOMO →LUMO +1 HOMO →LUMO +3	374.19	0.2580	32.36 % 6.40 % 3.45 % 4.08%

Table S5: Comparison of TDDFT data for [**CAD3**]$^+$**,** calculated using TD-B3LYP (6-31G(d)) and TD-CAM-B3LYP (6-31+G(d)) in dichloromethane using the polarisable continuum model (PCM) solvation model. Percentage contributions were calculated from %=200C^2, where C is the given contribution.

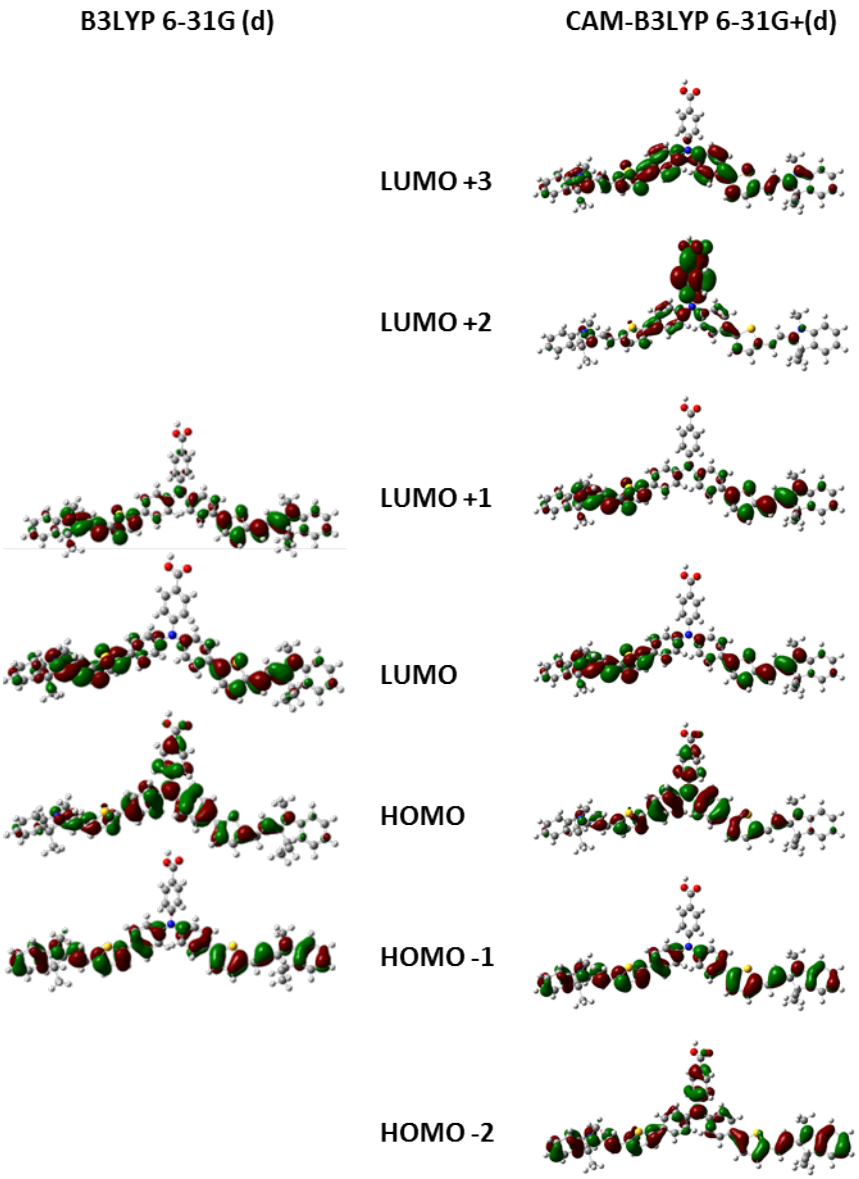

Figure S13. Comparison of the calculated electron distirbutions of the frontier molecular orbitals of [**CAD3**]$^+$**,** calculated using B3LYP (6-31G(d)) and CAM-B3LYP (6-31+G(d)) in dichloromethane using the polarisable continuum model (PCM) solvation model.

Key differences:

- B3LYP 6-31G(d) underestimates the energy of the electronic transitions whereas CAM-B3LYP 6-31G+(d) overestimates these transitions (compared with the experimentally obtained UV-Vis absorption spectra).
- For the two lower energy transitions (HOMO to LUMO and HOMO to LUMO +1), CAM-B3LYP calculated a small contribution from the HOMO -1 orbital to these transitions.
- For the highest energy transition, B3LYP assigned this transition as HOMO -1 to LUMO while CAM-B3LYP assigned this as having contributions from four different transitions, with HOMO -2 to LUMO being the predominant contribution.

Solar Cell Characterisation Data

NiO p-DSCs

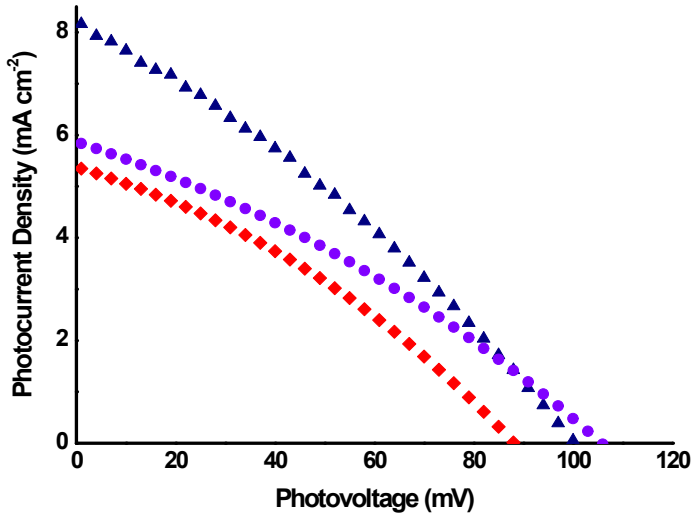

Figure S14. Current-voltage plots for NiO p-DSCs sensitized with the dyes **CAD3** (triangles), **GS1** (circles) and **P1** (diamonds), assembled with a platinised counter electrode and infiltrated with triiodide/iodide electrolyte.

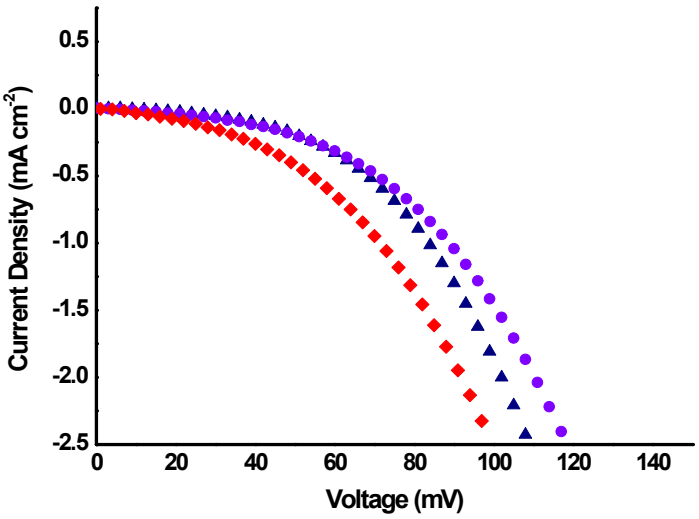

Figure S15. Dark current plots for NiO p-DSSCs sensitized with the dyes **CAD3** (triangles), **GS1** (circles) and **P1** (diamonds), assembled with a platinised counter electrode and infiltrated with triiodide/iodide electrolyte.

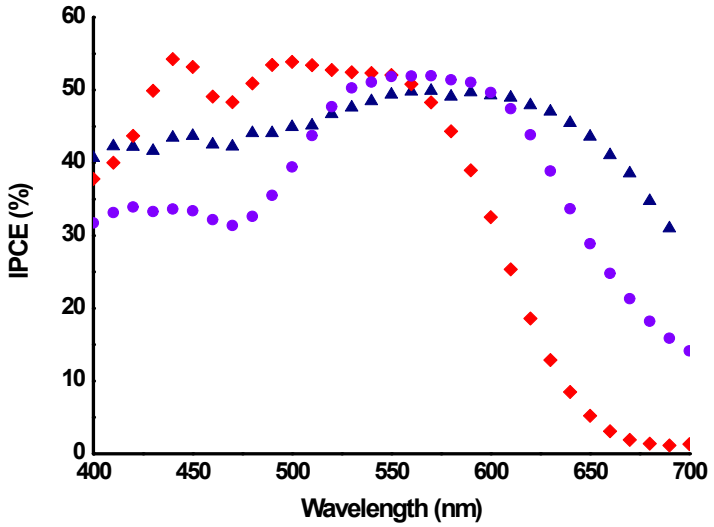

Figure S16. IPCE plots for NiO p-DSSCs sensitized with the dyes **CAD3** (triangles), **GS1** (circles) and **P1** (diamonds) assembled with a platinised counter electrode and infiltrated with triiodide/iodide electrolyte. The wavelength limit of our current experimental setup is 700 nm. CAD3 still exhibits an IPCE of ~30% at this wavelength and from the absorption spectrum in Figure S7 we anticipate that the spectral response should extend to 800 nm.

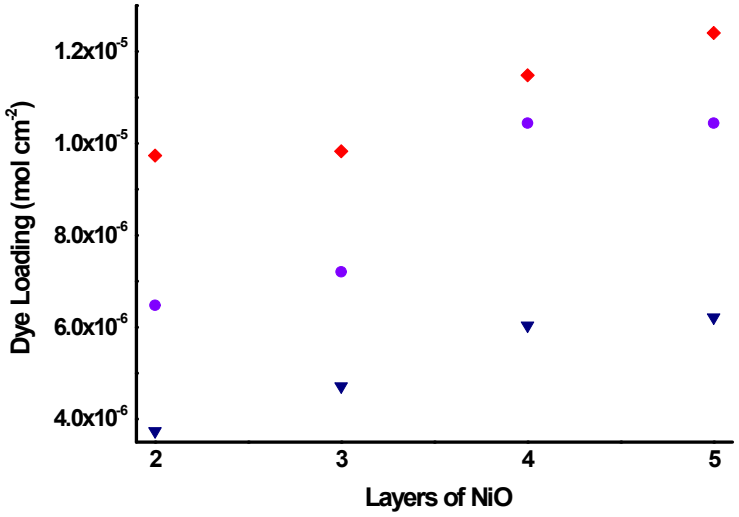

Figure S17. Dye loading plots for multi-layered NiO films sensitized with the dyes **CAD3** (triangles), **GS1** (circles) and **P1** (diamonds).

TiO_2 n-DSCs

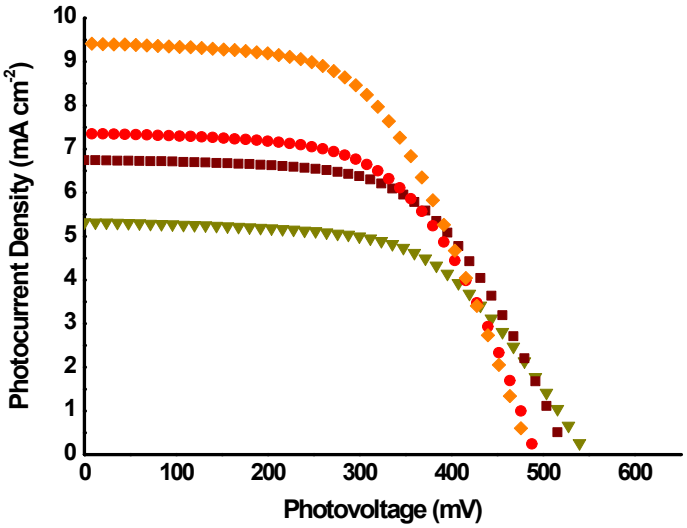

Figure S18. Current-voltage plots for TiO_2 n-DSCs sensitized with the dye **D35** using different dilutions of commercial TiO_2 paste in ethanol, **2(EtOH):1(TiO_2 paste)** (diamonds), **2.5:1** (circles), **3:1** (squares), **3.5:1** (triangles) assembled with a platinised counter electrode and infiltrated with triiodide/iodide electrolyte.

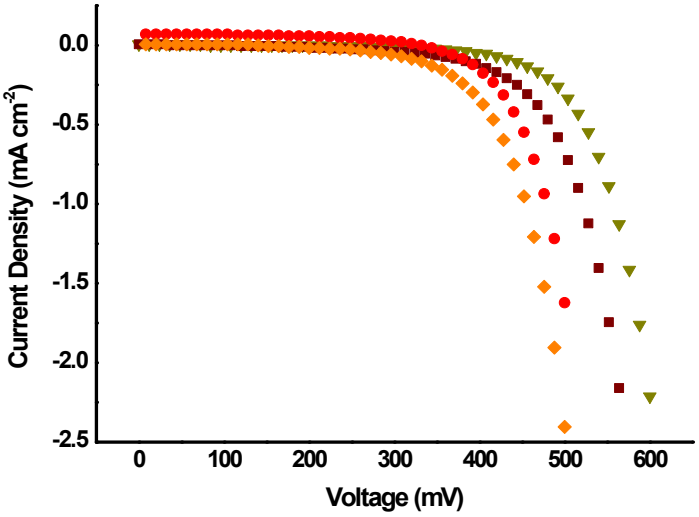

Figure S19. Dark current plots for TiO_2 n-DSSCs sensitized with the dye **D35** using different dilutions of commercial TiO_2 paste in ethanol, **2(EtOH):1(TiO_2 paste)** (diamonds), **2.5:1** (circles), **3:1** (squares), **3.5:1** (triangles), assembled with a platinised counter electrode and infiltrated with triiodide/iodide electrolyte.

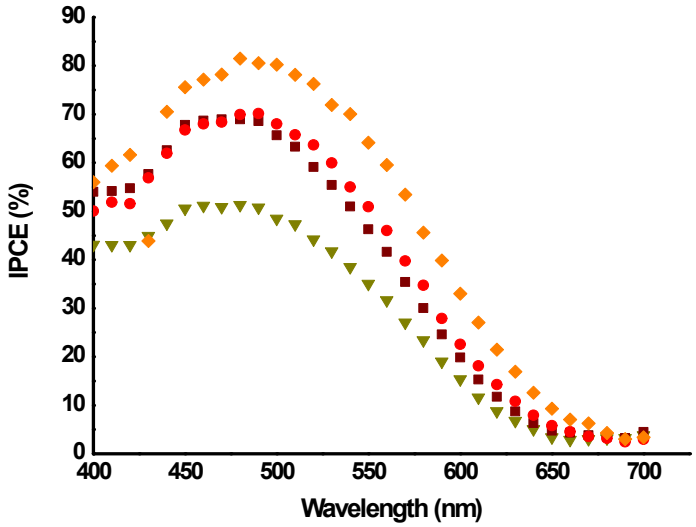

Figure S20. IPCE plots for TiO_2 n-DSSCs sensitized with the dye **D35** using different dilutions of commercial TiO_2 paste in ethanol, **2(EtOH):1(TiO_2 paste)** (diamonds), **2.5:1** (circles), **3:1** (squares), **3.5:1** (triangles), assembled with a platinised counter electrode and infiltrated with triiodide/iodide electrolyte.

Tandem DSCs

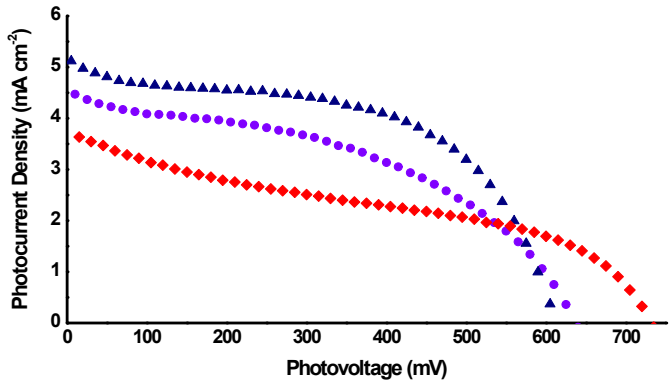

Figure S21. Current-voltage plots for for Tandem DSCs sensitized by D35/CAD 3 (triangles), D35/GS01 (circles) and D35/P1 (diamonds)

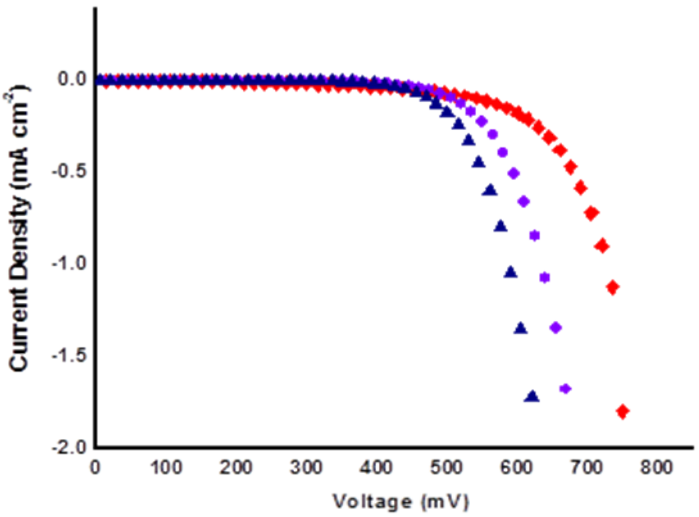

Figure S22. Dark current plots for Tandem DSCs sensitized by **D35/CAD3** (triangles), **D35/GS1** (circles) and **D35/P1** (diamonds).

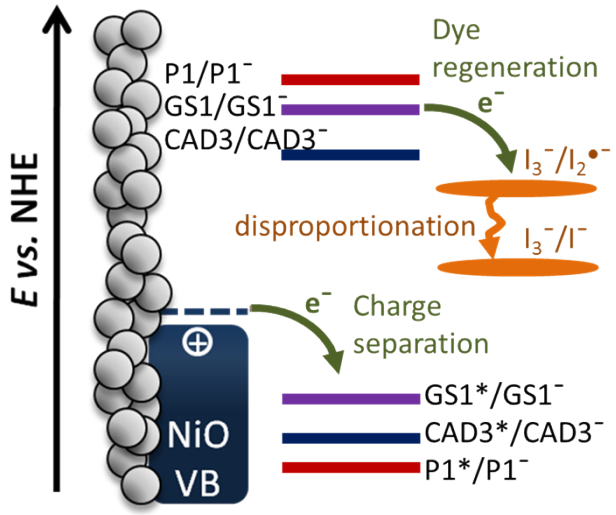

Figure S23. Relative potential energy levels of **P1**, **GS1**, **CAD3**.

References

[1] S. Sumikura, S. Mori, S. Shimizu, H. Usami, E. Suzuki, *J. Photochem. Photobiol.* **2008,** *199,* 1

[2] P. Qin, H. Zhu, T. Edvinsson, G. Boschloo, A. Hagfeldt, L. Sun. *J. Am. Chem. Soc.* **2008,** *130,* 8570

[3] M. Bielawski, M. Zhu, B Olofsson, *Adv. Synth. Catal.* **2007**, *349*, 2610

[4] J. Wen, R. Zhang, S. Chen, J. Zhang, X. Yu, *J. Org. Chem.* **2012**, *77*, 766

[5] A. R. Tyler, A. O. Okoh, C. L. Lawrence, V. C. Jones, C. Moffatt and R. B. Smith, *Eur. J. Med. Chem.*, **2013**, *64*, 222–7.

[6] Gaussian 03, Revision C.02, M. J. Frisch, G. W. Trucks, H. B. Schlegel, G. E. Scuseria, M. A. Robb, J. R. Cheeseman, J. A. Montgomery, Jr., T. Vreven, K. N. Kudin, J. C. Burant, J.

M. Millam, S. S. Iyengar, J. Tomasi, V. Barone, B. Mennucci, M. Cossi, G. Scalmani, N. Rega, G. A. Petersson, H. Nakatsuji, M. Hada, M. Ehara, K. Toyota, R. Fukuda, J. Hasegawa, M. Ishida, T. Nakajima, Y. Honda, O. Kitao, H. Nakai, M. Klene, X. Li, J. E. Knox, H. P. Hratchian, J. B. Cross, V. Bakken, C. Adamo, J. Jaramillo, R. Gomperts, R. E. Stratmann, O. Yazyev, A. J. Austin, R. Cammi, C. Pomelli, J. W. Ochterski, P. Y. Ayala, K. Morokuma, G. A. Voth, P. Salvador, J. J. Dannenberg, V. G. Zakrzewski, S. Dapprich, A. D. Daniels, M. C. Strain, O. Farkas, D. K. Malick, A. D. Rabuck, K. Raghavachari, J. B. Foresman, J. V. Ortiz, Q. Cui, A. G. Baboul, S. Clifford, J. Cioslowski, B. B. Stefanov, G. Liu, A. Liashenko, P. Piskorz, I. Komaromi, R. L. Martin, D. J. Fox, T. Keith, M. A. Al-Laham, C. Y. Peng, A. Nanayakkara, M. Challacombe, P. M. W. Gill, B. Johnson, W. Chen, M. W. Wong, C. Gonzalez, and J. A. Pople, Gaussian, Inc., Wallingford CT, 2004.

[7] Gaussian 09, Revision D.01, Frisch, M. J.; Trucks, G. W.; Schlegel, H. B.; Scuseria, G. E.; Robb, M. A.; Cheeseman, J. R.; Scalmani, G.; Barone, V.; Mennucci, B.; Petersson, G. A.; Nakatsuji, H.; Caricato, M.; Li, X.; Hratchian, H. P.; Izmaylov, A. F.; Bloino, J.; Zheng, G.; Sonnenberg, J. L.; Hada, M.; Ehara, M.; Toyota, K.; Fukuda, R.; Hasegawa, J.; Ishida, M.; Nakajima, T.; Honda, Y.; Kitao, O.; Nakai, H.; Vreven, T.; Montgomery, J. A., Jr.; Peralta, J. E.; Ogliaro, F.; Bearpark, M.; Heyd, J. J.; Brothers, E.; Kudin, K. N.; Staroverov, V. N.; Kobayashi, R.; Normand, J.; Raghavachari, K.; Rendell, A.; Burant, J. C.; Iyengar, S. S.; Tomasi, J.; Cossi, M.; Rega, N.; Millam, M. J.; Klene, M.; Knox, J. E.; Cross, J. B.; Bakken, V.; Adamo, C.; Jaramillo, J.; Gomperts, R.; Stratmann, R. E.; Yazyev, O.; Austin, A. J.; Cammi, R.; Pomelli, C.; Ochterski, J. W.; Martin, R. L.; Morokuma, K.; Zakrzewski, V. G.; Voth, G. A.; Salvador, P.; Dannenberg, J. J.; Dapprich, S.; Daniels, A. D.; Farkas, Ö.; Foresman, J. B.; Ortiz, J. V.; Cioslowski, J.; Fox, D. J. Gaussian, Inc., Wallingford CT, 2009.

[8] Kobayashi, R., & Amos, R. D. *Chem. Phys. Lett.* **2006**, *420*, 106–109.